GLOBAL L-BAND VEGETATION VOLUME FRACTION ESTIMATES FOR MODELING VEGETATION OPTICAL DEPTH

David Chaparro[1,], Thomas Jagdhuber[2,3], María Piles[4], Dara Entekhabi[5], François Jonard[6,7], Anke Fluhrer[2,3], Andrew Feldman[5], Mercè Vall-llossera[1], Adriano Camps[1]*

[1]Universitat Politècnica de Catalunya, CommSensLab & IEEC-UPC, Jordi Girona 1-3, 08034 Barcelona, Spain.
[2]German Aerospace Center, Microwaves and Radar Institute, Muenchener Strasse 20, 82234 Weßling, Germany.
[3]University of Augsburg, Institute of Geography, Alter Postweg 118, 86159 Augsburg.
[4]Image Processing Laboratory (IPL), Universitat de València, 46010 València, Spain.
[5]Department of Civil and Environmental Engineering, Massachusetts Institute of Technology, Cambridge, MA 02139, USA.
[6]Agrosphere (IBG-3), Institute of Bio- and Geosciences, Forschungszentrum Jülich GmbH, Germany.
[7]Geomatics Unit, Université de Liège, 4000 Liège, Belgium.
*Contact author: david.chaparro@tsc.upc.edu

IGARSS 2021 - 2021 IEEE International Geoscience and Remote Sensing Symposium | 978-1-6654-0369-6/21/$31.00 ©2021 IEEE | DOI: 10.1109/IGARSS47720.2021.9554872

ABSTRACT

The attenuation of microwave emissions through the canopy is quantified by the vegetation optical depth (VOD), which is related to the amount of water, the biomass and the structure of vegetation. To provide microwave-derived plant water estimates, one must account for biomass/structure contributions in order to extract the water component from the VOD. This study uses Aquarius scatterometer data to build an L-band global seasonality of vegetation volume fraction (δ), representative of biomass/structure dynamics. The dynamic range of δ is adapted for its application in a gravimetric moisture (Mg) retrieval model. Results show that δ ranging from 0 to $3.35 \cdot 10^{-4}$ is needed for modelling physically reasonable Mg values. The global average of δ shows consistent spatial patterns across vegetation distributions, and δ seasonality is coherent with the phenology of the studied vegetation types. These findings enable the separation of information on vegetation water and biomass/structure inherent within VOD.

Index Terms— Vegetation structure, vegetation gravimetric moisture content, biomass, Aquarius scatterometer.

1. INTRODUCTION

The vegetation water content is a key variable linking the water and carbon cycles. Hence, an accurate retrieval of vegetation hydric conditions is essential to monitor the plant water fluxes and the vegetation responses to climate change.

L-band passive microwave sensors on board of the ESA's Soil Moisture and Ocean Salinity (SMOS) mission and the NASA's Soil Moisture Active-Passive (SMAP) mission are sensitive to the water content of the full canopy layer through the attenuation parameter "vegetation optical depth" (VOD). Nevertheless, as the VOD is also sensitive to the structure and biomass of plants, there is a need of disentangling water from biomass/structure contributions to this parameter, especially in regions with high biomass dynamics (e.g., croplands).

An attenuation-based approach was proposed in [1] and [2] to retrieve the water component of VOD as the gravimetric moisture of vegetation (Mg; [kg water/kg biomass]). Mg represents the water in plants independently of other characteristics (e.g., biomass) and is more closely related to the actual water status than the area-based vegetation water content (VWC) [2]. Following [1] and [2], Mg estimates can be obtained by minimizing the differences between radiometer-based and modeled VOD. Hence, the Mg-estimation relies on the modeling of VOD, for which the following physical formulation is proposed [3]:

$$VOD = 4\pi \frac{VH}{\lambda} \cdot Im[\sqrt{\varepsilon_{can}}] \quad (1).$$

The input variables to this model are the vegetation height (VH), the wavelength (λ=21 cm at 1.4 GHz) and the dielectric constant of the canopy (ε_{can}), which is in turn estimated by dielectric models (Section 2.2.2) requiring the microwave-based parameter "vegetation volume fraction" (δ).

The δ parameter is the fraction of vegetation "seen" by a microwave remote sensing acquisition scenario. It is derived here from the radar vegetation indices (RVI) [1] and represents the volume proportion of solid vegetation material in air. It accounts for vegetation structure and dry biomass. Due to the phenological variability in biomass and structure existing in many regions, it is essential to account for these components when estimating Mg. Previously, δ–estimates at L-band have been obtained as constant values from a global SMAP radar 3-month average [1], and both as constants and as dynamic parameters from field-scale measurements [2]. In both cases, the dynamic range of δ varied depending on the model used for ε_{can} estimation.

In this context, this work aims at providing global maps and seasonality of δ as a necessary step towards gravimetric

plant water status monitoring with SMAP. Two specific goals are proposed: (i) to define the dynamic range of δ needed for realistic Mg estimation by choosing the appropriate ε_{can} model; and (ii) to provide a global seasonality of δ from L-band scatterometer data and compare it with the global distribution of vegetation patterns and with the phenology of representative regions.

2. DATA AND METHODS

2.1. Data

2.1.1. Aquarius radar backscatter

Despite its coarse resolution (~100 km), the Aquarius/SAC-D mission is the best suited in terms of multi-year coverage and adequate temporal sampling (revisit time is ~7 days) to obtain regional-scale seasonality of the δ-parameter. The L-band active scatterometer on board of Aquarius provided polarimetric (HH, VV, VH) backscattering (σ) data between years 2011 and 2014, which are used in this study. For consistency, only the central beam at incidence angle θ_i=~38º is used, which is similar to the SMAP incidence angle (θ_i=40º). Note that the δ estimates should be applicable for future SMAP-derived gravimetric moisture estimates. The Aquarius spatial resolution for the central beam is 84 x 120 km. Values represent the center of Aquarius pixels, and they are aggregated to match the 9 km SMAP EASE2 grid. This will ease future combination with VOD products. The data is first screened out for very low values of backscatter (σ<-40 dB), and then transformed from dB to linear units.

2.1.2. Auxiliary data

Land Cover (LC) data from the MODIS International Geosphere-Biosphere Programme (IGBP, MCD12C1 product v.6; 3 km resolution) is aggregated by modal classes to the 9 km gridding. LC will be used to define focus regions.

Vegetation height (VH) is obtained from [4] and aggregated to the 9 km EASE grid. It will be applied for VOD modelling in Section 2.2.2.

2.2. Methods

2.2.1. Computation of δ

As a first step for obtaining δ and following the approach in [1], the RVI is calculated as follows:

$$\mathrm{RVI} = \frac{8 \cdot \sigma_{\mathrm{HV}}}{\sigma_{\mathrm{HH}} + \sigma_{\mathrm{VV}} + 2 \cdot \sigma_{\mathrm{HV}}} \quad (2),$$

where σ_{HV}, σ_{HH}, and σ_{VV} are the normalized backscattering coefficients at cross- and co-polarizations. Unexpected RVI values (RVI>1) have been screened out (i.e., <2% of data). Afterwards, RVI ranges between 0 and 1. Secondly, a constant k is used to rescale the RVI to an appropriate dynamic range and obtain δ:

$$\delta = k \cdot \mathrm{RVI} \quad (3).$$

2.2.2. Estimating the dynamic range of δ by ε_{can}-modelling

The imaginary part of ε_{can} is an essential component of the VOD model (Eq. 1) which is used for Mg-estimation in [1] and [2]. According to [5], ε_{can} can be expressed as:

$$\varepsilon_{can} = \varepsilon_{host} + \frac{\delta}{3}\left(\varepsilon_{veg} - \varepsilon_{host}\right) \sum_{u=a,b,c} \left(\frac{1}{1 + A_u \left(\frac{\varepsilon_{veg}}{\varepsilon_{host}} - 1 \right)} \right) \quad (4),$$

where ε_{host} = 1 (air is the host medium), and a range of values between 0 and 15 is assigned to the imaginary part of the dielectric constant of vegetation (ε_{veg}). The parameter A_u is the shape or depolarization factor and describes the influence of the inclusion shapes on ε_{can}. These inclusions simulate leaves as ellipsoids [5,6]. Defining their semi-axes values (a, b and c) leads to: (i) different assumptions of leaves shapes (Table 1), and (ii) changes in the dynamic ranges of the resulting variables (ε_{can} and, subsequently, VOD estimates). These changes must be counterbalanced by modifying the constant k in the δ calculation (Eq. 3). In that sense, k (and consequently the range of δ) need to be determined by constraining VOD and VH to maximum physically-reasonable/useful values, independently of the assumed inclusions. In that sense, Table 1 shows k values proposed in this work to modulate the δ range for each inclusion shape while keeping VOD outputs and VH inputs between 0 and their 99.9th percentile ($VOD_{P99.9}$ = 2; $VH_{P99.9}$ = 40 m). Lower percentiles were found to be too restrictive, excluding values that cannot be considered as outliers (e.g., VOD_{P99}<1.5; VH_{P99}<40 m).

Table 1. Shapes of the inclusions, depolarization factor for each semi-axis (a, b and c), and value of k in Eq. (4) [5,6].

Inclusions	A_a	A_b	A_c	k
Spheres (s)	1/3	1/3	1/3	$6.1 \cdot 10^{-3}$
Random needles (rn)	0.5	0.5	0	$3.35 \cdot 10^{-4}$
Random disks (rd)	0	0	1	$1.68 \cdot 10^{-4}$

As examples of the impacts of δ and shape inclusions on VOD estimates, values in Table 1 are applied to a tropical forest pixel (2.93ºN, 115.07ºW; VH=39 m) and to a woody savanna pixel (13.43ºS, 23.11ºE; VH=12 m). In these examples, the full range of possible VOD estimates is calculated as a function of δ and ε_{veg} by using (1) and (4).

2.2.3. Delta maps and seasonality

As a first step to establish the δ seasonality, the three years of Aquarius data are averaged and smoothed. Smoothing is done by using a Savitzky-Golay filter (2nd degree polynomial; 61-

day window). Secondly, regions without data (i.e., mainly those not covered by the central beam of Aquarius) are filled using a spatial moving window (inverse distance weighted averaging) of size three-fold the Aquarius resolution (i.e., 27 x 39 EASE 9 km pixels).

Four focus regions with different and homogeneous land cover types (grasslands, croplands, woody savannah and tropical forests; Fig. 2) are chosen to study the δ seasonality.

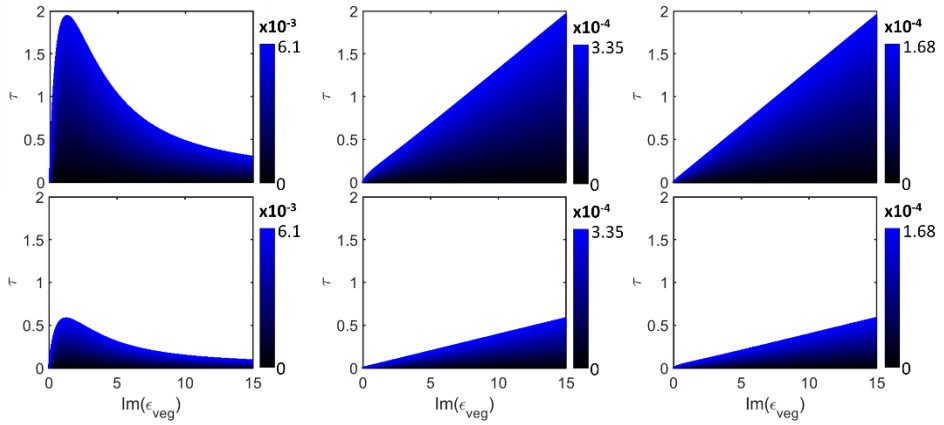

Fig. 1. Modelled τ (VOD) as a function of δ (colorbar; note the different dynamic ranges) and ε_{veg} for different inclusions: spheres (left), random needles (centre) and random disks (right). Top row: tropical forest pixel (2.93ºN, 115.07ºW; VH=39 m). Bottom row: woody savannah pixel (13.43ºS, 23.11ºE; VH=12 m).

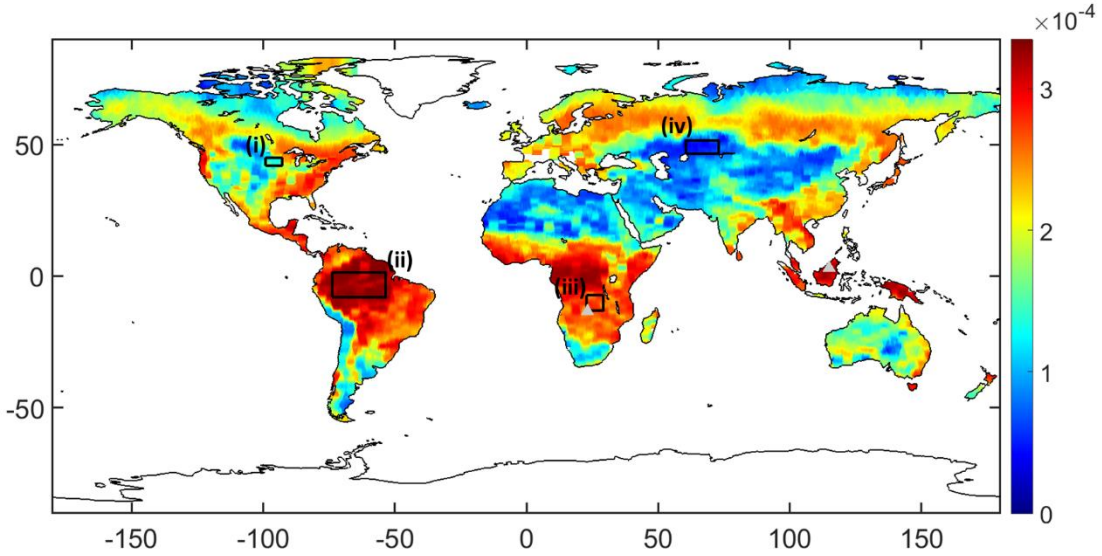

Fig.2. Global map of δ seasonality. Four focus regions are outlined (black boxes): (i) croplands, (ii) tropical forests, (iii) woody savannas, and (iv) grasslands. The two pixels studied in Fig. 1 are highlighted with grey triangles.

3. RESULTS AND DISCUSSION

3.1. ε_{can} models and δ dynamic range

Figure 1 shows the results of VOD estimates using the full ranges of ε_{veg} (0 to 15) and δ-values. Dynamic ranges of δ are adapted to keep the same physical ranges for the output variable (VOD, or τ) for the three inclusions studied (spheres, random needles, and random disks). Also, Fig. 1 shows that the shape and trends of the spheres inclusion model is opposite to those from needles and disks.

In particular, the spheres model shows increasing VOD values for decreasing dielectric constant of vegetation (Fig. 1). This suggests that assuming spheres inclusions is not appropriate as it lacks physical sense: increasing attenuation should be related to increasing water content (here represented by ε_{veg}). In contrast, random needles and disks show similar results with VOD and ε_{veg} being positively correlated, as expected. This finding adapts the method proposed in [1] by modifying the assumptions on vegetation inclusions and represents a step forward for global plant water retrievals based on this approach. Finally, random

needles inclusions are assumed for subsequent analyses and δ will range between 0 and $3.35 \cdot 10^{-4}$ (as $k = 3.35 \cdot 10^{-4}$).

3.2. Map and seasonality of δ

The vegetation volume fraction is shown in Fig. 2 as an average map of δ seasonality (extracted from years 2011-2014). Note that the spatial patterns are consistent with the global distribution of vegetation. The highest δ values are found in regions with the largest biomass (i.e., in the tropics) while regions with low vegetation cover (e.g., grasslands) show δ values near 0. Also, middle to high δ values are found in boreal forests ($3 \cdot 10^{-4} < \delta < 4 \cdot 10^{-4}$) and savannas ($\delta > 4 \cdot 10^{-4}$).

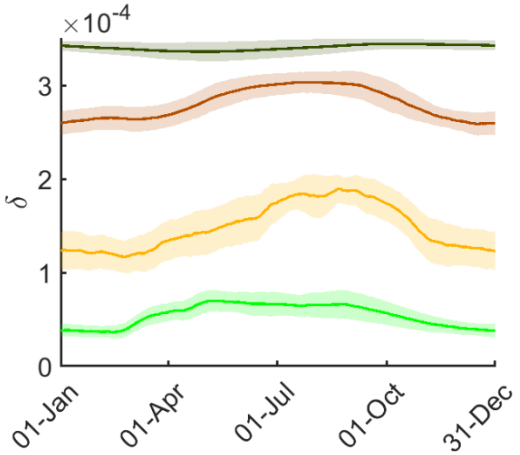

Fig. 3. Average (solid line) and +/- std (shaded area) of δ in each of the studied regions, highlighted in Fig. 2.

Figure 3 shows the estimated annual seasonality of δ for the regions highlighted in Fig. 2. The expected pattern of increasing δ with larger vegetation cover is also seen here. The lowest temporal variability of δ is found for tropical forests, where vegetation biomass is rather constant throughout the year and where plants are evergreen. The strongest dynamics are found in woody savannas and in croplands. In both cases, time-patterns match the vegetation phenology in these regions and are consistent with the annual plant cycle detected by other sensors and variables (e.g., [7,8]). Grasslands in central Asia show smaller variability in absolute terms, although their changes are large in relative terms: the spring-summer plateau of δ is ~50% larger than the minimum of winter values.

In conclusion, both spatial and temporal trends for δ match the expected behavior by detecting the different land cover patterns on the globe. Also, the retrieved spatio-temporal patterns of δ capture the expected magnitude and periods of biomass/structure changes in each of the studied regions which, in the context of water research, will be essential for gravimetric moisture retrieval algorithms. In addition, the capacity of δ to capture biomass and phenology suggests that VOD estimates proposed here can contribute to carbon stocks monitoring as well, especially when improved resolution for δ values is achieved in future missions.

3.3. Current and future L-band radar missions to improve spatial resolution of δ

Finally, note that, although global and regional spatial patterns are appreciated, the coarse spatial resolution of Aquarius does not allow to inform about local details. Hence, future research should address currently acquired L-band SAR data from ALOS-PALSAR or SAOCOM missions. Nevertheless, in these missions the restrictions in temporal revisit, data availability (restricted access) or still short data periods (SAOCOM: launched on October 2018) hamper creating a dynamic δ dataset. Furthermore, future L-band SAR missions such as NISAR (~2022) and ROSE-L (~2028) may provide high spatial resolution for retrieving full canopy vegetation volume fraction information.

4. ACKNOWLEDGEMENTS

This work was supported by "la Caixa" Foundation (ID 100010434), under agreement LCF/PR/MIT19/51840001 (MIT-Spain Seed Fund), and by the Spanish Ministry of Science, Innovation and Universities and the European Regional Development Fund (ERDF, EU) through projects ESP2017-89463-C3-3-R, RTI2018-096765-A-100, CAS19/00264 and MDM-2016-0600. Also, the authors are grateful to MIT for supporting this research with the MIT-Germany Seed Fund (D. Entekhabi, T. Jagdhuber).

5. REFERENCES

[1] Fink, A., Jagdhuber, T., Piles, M., Grant, J., Baur, M., Link, M., & Entekhabi, D. (2018, July). Estimating gravimetric moisture of vegetation using an attenuation-based multi-sensor approach. In IGARSS 2018-*2018 IEEE International Geoscience and Remote Sensing Symposium* (pp. 353-356). IEEE.

[2] Meyer, T., Jagdhuber, T., Piles, M., Fink, A., Grant, J., Vereecken, H., & Jonard, F. (2019). Estimating gravimetric water content of a winter wheat field from L-band vegetation optical depth. *Remote Sensing, 11*(20), 2353.

[3] Schmugge, T. J., & Jackson, T. J. (1992). A dielectric model of the vegetation effects on the microwave emission from soils. *IEEE Transactions on Geoscience and Remote Sensing, 30*(4), 757-760.

[4] Simard, M., Pinto, N., Fisher, J. B., & Baccini, A. (2011). Mapping forest canopy height globally with spaceborne lidar. *Journal of Geophysical Research: Biogeosciences, 116*(G4).

[5] Ulaby, F.T., Long, D.G., Blackwell,W.J., Elachi, C., Fung, A.K., Ruf, C., Sarabandi, K., Zebker, H.A., Van Zyl, J. Microwave Radar and Radiometric Remote Sensing; University of Michigan Press: Artech House, MI, USA, 2014.

[6] Loor,G.D. (1968). Dielectric properties of heterogeneous mixtures containing water. Journal of Microwave Power,3(2),67-73.

[7] Chaparro, D., Piles, M., Vall-Llossera, M., Camps, A., Konings, A. G., & Entekhabi, D. (2018). L-band vegetation optical depth seasonal metrics for crop yield assessment. *Remote Sensing of Environment, 212*, 249-259.

[8] Tian, F., Wigneron, J. P., Ciais, P., Chave, J., Ogée, J., Penuelas, J., ... & Mialon, A. (2018). Coupling of ecosystem-scale plant water storage and leaf phenology observed by satellite. *Nature Ecology & Evolution, 2*(9), 1428-1435.